IOP Publishing Plasma Physics and Controlled Fusion
Plasma Phys. Control. Fusion **65** (2023) 105005 (11pp) https://doi.org/10.1088/1361-6587/aceb88

Verification of gyrokinetic particle simulations of neoclassical tearing modes in fusion plasmas

Kaijie Wang[1,9], Shuying Sun[1,2,3,9], Wenlu Zhang[4,5,6,*], Zhihong Lin[2,*], Xishuo Wei[2], Pengfei Liu[2], Hongying Feng[4,5,6,7], Xiaogang Wang[8] and Ding Li[4,5,6]

[1] Fusion Simulation Center, Peking University, Beijing 100871, People's Republic of China
[2] Department of Physics and Astronomy, University of California, Irvine, CA 92697, United States of America
[3] China Academy of Aerospace Science and Technology Innovation, Beijing 100176, People's Republic of China
[4] Beijing National Laboratory for Condensed Matter Physics and CAS Key Laboratory of Soft Matter Physics, Institute of Physics, Chinese Academy of Sciences, Beijing 100190, People's Republic of China
[5] University of Chinese Academy of Sciences, Beijing 100049, People's Republic of China
[6] Department of Modern Physics, University of Science and Technology of China, Hefei, Anhui 230026, People's Republic of China
[7] College of Mechanical and Power Engineering, China Three Gorges University, Yichang, Hubei 443002, People's Republic of China
[8] Laboratory for Space Environment and Physics Sciences, Harbin Institute of Technology, Harbin 150001, People's Republic of China

E-mail: wzhang@iphy.ac.cn and zhihongl@uci.edu

Received 10 March 2023, revised 6 July 2023
Accepted for publication 28 July 2023
Published 29 August 2023

Abstract
The ability to simulate neoclassical tearing modes (NTMs) in the gyrokinetic toroidal code (GTC) has been developed and verified, in which ions are treated with a gyrokinetic model and electrons are treated as a resistive fluid. The simulation results demonstrate that the neoclassical bootstrap current effect can destabilize an otherwise stable classical tearing mode. In the cylindrical geometry, GTC simulations in the magnetohydrodynamic limit show quantitative agreement with the modified Rutherford theory, both in terms of the scaling law in the small island limit and in terms of the saturation level and pressure flattening effect in the large island limit. The toroidal effects are slightly destabilizing for the NTM, while the kinetic effects of thermal ions are stabilizing for the NTM and increase its excitation threshold.

Keywords: neoclassical tearing modes (NTM), gyrokinetic simulation, ion kinetic effects

(Some figures may appear in colour only in the online journal)

1. Introduction

In tokamak experiments, current-driven tearing mode (TM) due to finite resistivity can tear the magnetic surface and form islands around a rational flux surface. This TM instability is determined by the classical tearing stability index Δ' [1, 2]. However, the pressure profile can be flattened inside the island. As a result, the bootstrap current inside the island vanishes, leading to further growth of the island [3, 4]. This instability is called the neoclassical TM (NTM). NTM islands can limit achievable normalized plasma pressure, degrade plasma confinement and damp plasma rotation. Most importantly, NTMs are considered the most likely instabilities leading to

[9] These authors contributed equally to this work.
[*] Authors to whom any correspondence should be addressed.

disruption in many tokamak experiments [5, 6]. Thus, gaining a comprehensive understanding of NTM physics remains an important objective for tokamak research [7].

NTMs have been studied in fusion plasmas for several decades. The modified Rutherford equation (MRE) [2, 8, 9] including the perturbed bootstrap current term is a theory most commonly used to describe the behavior of the NTMs. This equation predicts that a magnetic island of finite width is needed to excite an NTM and that the magnetic island can naturally saturate at a certain width. Some NTM simulations have been performed in the magnetichydrodynamic (MHD) framework, including simulations using TM8 [10], XTOR [11], NIMROD [12] and MDC [13], which agree well with the theoretical prediction. These MHD codes incorporate the effect of the bootstrap current by means of an additional pressure diffusion equation. However, the kinetic effects of thermal ions can be significant for the evolution of NTM islands. On one hand, the bootstrap current intrinsically comes from the kinetic effects. On the other hand, the finite orbit width may reduce the bootstrap current drive by partially maintaining the pressure gradient across a small island. Thus, the simplified models in these MHD codes limit their accuracy and reliability, which calls for first-principle gyrokinetic simulations.

Furthermore, in high-temperature tokamak discharges, energetic particles from auxiliary heating and fusion products could be significant components of plasma pressures and influence the dynamics of NTM islands. Several experiments [14–16] have demonstrated that magnetic islands can impact the transport of fast ions, which could affect plasma heating and heat loading on the first wall. The destabilization or stabilization of an NTM by the redistribution of fast ions has also been reported [17]. Despite the progress made to several aforementioned MHD codes to incorporate the kinetic effects of energetic particles and reproduce experimental observations [18], the interaction between fast particles and NTM islands has not been well understood. Therefore, a self-consistent study of the interaction between NTMs and energetic particles also requires gyrokinetic simulations.

For the above reasons, we have further developed the gyrokinetic toroidal code (GTC) [19] for first-principle simulations of NTMs. GTC has been extensively applied to study neoclassical and turbulent transport [20, 21], energetic particles [22] and Alfven eigenmodes [23–25]. In previous work, the implementation of equilibrium current [26] enables simulations of current-driven instabilities in the toroidal geometry with kinetic effects, including the kink modes [27, 28], resistive TMs [29], collisionless TMs [30] and drift TMs [31].

As the first step attempting to simulate the NTM via a first-principle approach, we will not attempt to cover all neoclassical effects in this study, but instead focus on the most important one, i.e. the bootstrap current effect with finite parallel thermal diffusivity. To capture this effect, we have extended the GTC formulations [26, 32] to simulate NTMs in fusion plasmas by adding the bootstrap current effect in Ohm's law via standard neoclassical model and an additional pressure evolution equation based on a diffusion model. This NTM simulation model is first verified in cylindrical geometry simulations in the MHD limit. Our results demonstrate that, the neoclassical bootstrap current effect can destabilize an otherwise stable classical TM. Simulations in the small island limit show a linear increase in the NTM growth rate with poloidal beta, in quantitative agreement with the modified Rutherford theory. Nonlinear simulations of the NTM evolution also show good agreement with the MRE in terms of saturation level and maximum growth. We have also performed simulations in a toroidal geometry and found that toroidal geometry can have a destabilizing effect on NTMs. Gyrokinetic simulations in the toroidal geometry show that the kinetic effects of thermal ions can significantly reduce the NTM growth rate for the small island width, despite the destabilizing effect of the toroidicity. These findings suggest that the kinetic effects of thermal ions play a vital role in determining the threshold for the NTM excitation [9, 33, 34].

This paper is organized as follows. In section 2, the NTM simulation model is formulated. We first derive our NTM simulation model with gyrokinetic ions and fluid electrons and then simplify it to a reduced MHD description. In section 3, the NTM simulations in the MHD limit are described and verified against the MRE. The toroidal effects and thermal ion kinetic effects on the NTM stability are discussed in sections 4 and 5, respectively. Finally, the summary and conclusions are presented in section 6.

2. Gyrokinetic model for NTM simulation

Prior research [26, 29, 31, 35] has established a gyrokinetic model suitable for classical TMs. This model treats ions with gyrokinetics, while electrons are modeled as a massless fluid. For the present work on NTM simulations, we have extended this model by incorporating the bootstrap current effect into Ohm's law and using an additional pressure transport equation. By combining this with Ampere's law and the Poisson equation, we have established a comprehensive electromagnetic system that is well-suited for NTM simulations.

2.1. Gyrokinetic model for ions

We begin with the collisionless gyrokinetic equations with an inhomogeneous magnetic field [36]:

$$\frac{\mathrm{d}}{\mathrm{d}t}f_\alpha\left(\boldsymbol{R},\mu,v_\parallel,t\right)=\left(\frac{\partial}{\partial t}+\dot{\boldsymbol{R}}\cdot\nabla+\dot{v}_\parallel\frac{\partial}{\partial v_\parallel}\right)f_\alpha=0, \tag{1}$$

$$\dot{\boldsymbol{R}}=v_\parallel\boldsymbol{b}_0+v_\parallel\frac{\delta\boldsymbol{B}_\perp}{B^*_\parallel}+\boldsymbol{v}_{\boldsymbol{E}}+\boldsymbol{v}_{\boldsymbol{g}}+\boldsymbol{v}_{\boldsymbol{c}}, \tag{2}$$

$$\dot{v}_\parallel=-\frac{1}{m_\alpha}\frac{\boldsymbol{B}^*}{B^*_\parallel}\cdot\left(\mu\nabla B_0+q_\alpha\nabla\phi\right)-\frac{q_\alpha}{m_\alpha c}\frac{\partial A_\parallel}{\partial t}, \tag{3}$$

where

$$\boldsymbol{B}^*=\boldsymbol{B}_0+\frac{B_0v_\parallel}{\Omega_\alpha}\nabla\times\boldsymbol{b}_0+\delta\boldsymbol{B}_\perp,\ B^*_\parallel=B_0+\frac{B_0v_\parallel}{\Omega_\alpha}\boldsymbol{b}_0\cdot\nabla\times\boldsymbol{b}_0\ . \tag{4}$$

The index α indicates different particle species (i for ions or e for electrons). f_α is the distribution function for species α. $\boldsymbol{R}$, μ, $v_\parallel$, m_α, q_α and $\Omega_\alpha = q_\alpha B_0/m_\alpha c$ are the particle guiding center, magnetic moment, parallel particle velocity, particle mass, particle charge, and cyclotron frequency, respectively. $\boldsymbol{b}_0 = \boldsymbol{B}_0/B_0$ is the unit vector in the magnetic direction. The drift velocities include the electric drift velocity $\boldsymbol{v_E}$, magnetic gradient drift velocity $\boldsymbol{v_g}$, and curvature drift velocity $\boldsymbol{v_c}$,

$$\begin{aligned}\boldsymbol{v_E} &= c\boldsymbol{b}_0 \times \nabla\phi/B_\parallel^*,\\ \boldsymbol{v_g} &= \mu\boldsymbol{b}_0 \times \nabla B_0/\left(m_\alpha\Omega_\alpha\right),\\ \boldsymbol{v_c} &= v_\parallel^2\nabla\times\boldsymbol{b}_0/\Omega_\alpha.\end{aligned}$$

The force in the parallel direction includes the mirror force and the electric field force. The compressional component of the perturbed magnetic field is neglected in this work and will be included in future study. Assuming that there is no equilibrium electric field, ϕ and $A_\parallel$ can be replaced by their perturbed parts $\delta\phi$ and $\delta A_\parallel$, respectively, then $\delta\boldsymbol{B}_\perp$ can be written as $\delta\boldsymbol{B}_\perp = \nabla\times\delta A_\parallel\boldsymbol{b}_0$. We will use the magnetic flux coordinates (ψ,θ,ζ) for convenient of toroidal geometry simulations, where ψ is the poloidal flux, θ and ζ are poloidal and toroidal angles, respectively. Using this coordinates, the equilibrium magnetic field can be represented in the covariant and contravariant form as

$$\boldsymbol{B}_0 = \delta\nabla\psi + I\nabla\theta + g\nabla\zeta \tag{5}$$

$$= q\nabla\psi\times\nabla\theta - \nabla\psi\times\nabla\zeta. \tag{6}$$

For noise suppression, we choose the δf method [37] in our model. Equation (1) can be rewritten for the perturbed ion distribution as follows:

$$\begin{aligned}*20c\frac{\mathrm{d}w_\mathrm{i}}{\mathrm{d}t} = (1-w_\mathrm{i})\Bigg[&-\left(v_\parallel\frac{\delta\boldsymbol{B}_\perp}{B_\parallel^*}+\boldsymbol{v_E}\right)\cdot\frac{\nabla f_{0\mathrm{i}}}{f_{0\mathrm{i}}}\\ &+\left(\mu\frac{\delta\boldsymbol{B}_\perp}{B_\parallel^*}\cdot\nabla B_0 + q_\mathrm{i}\frac{\boldsymbol{B^*}}{B_\parallel^*}\cdot\nabla\delta\phi + \frac{q_\mathrm{i}}{c}\frac{\partial\delta A_\parallel}{\partial t}\right)\frac{1}{m_\mathrm{i}}\frac{1}{f_\mathrm{i}}\frac{\partial f_{0\mathrm{i}}}{\partial v_\parallel}\Bigg]\end{aligned} \tag{7}$$

where $w_\mathrm{i}\equiv\delta f_\mathrm{i}/f_\mathrm{i}$ is the particle weight for ions and $f_{0\mathrm{i}}$ is the equilibrium distribution function for ions. Equations (2)–(7) form the gyrokinetic model for ions.

2.2. Fluid model for electrons

In order to properly account for electron behavior at the MHD scale, we integrate equations (1)–(3) for electrons in velocity space to obtain the fluid equations for an NTM in the MHD limit. In the electron fluid limit, we retain the adiabatic part of the perturbed electron distribution. Assuming no equilibrium electric field and an equilibrium distribution function f_{e0} described by a shifted Maxwellian, we obtain the perturbed fluid continuity equation for electrons,

$$\begin{aligned}&\frac{\partial\delta n_\mathrm{e}}{\partial t} + \boldsymbol{B}_0\cdot\nabla\left(\frac{n_{0\mathrm{e}}\delta u_{\parallel\mathrm{e}}}{B_\parallel^*}\right) + B_0\boldsymbol{v_E}\cdot\nabla\left(\frac{n_{0\mathrm{e}}}{B_\parallel^*}\right)\\ &\quad - n_{0\mathrm{e}}\left(\delta\boldsymbol{v_{*e}}+\boldsymbol{v_E}\right)\cdot\frac{\nabla B_0}{B_\parallel^*} + \delta\boldsymbol{B}_\perp\cdot\nabla\left(\frac{n_{0\mathrm{e}}u_{\parallel 0\mathrm{e}}}{B_\parallel^*}\right)\\ &\quad + \frac{c\nabla\times\boldsymbol{B}_0}{B_\parallel^{*2}}\cdot\left(-\frac{\nabla\delta p_\mathrm{e}}{\mathrm{e}} + n_{0\mathrm{e}}\nabla\delta\phi\right)\\ &\quad + \Bigg[\delta\boldsymbol{B}_\perp\cdot\nabla\left(\frac{n_{0\mathrm{e}}\delta u_{\parallel\mathrm{e}}}{B_\parallel^*}\right) + B_0\boldsymbol{v_E}\cdot\nabla\left(\frac{\delta n_\mathrm{e}}{B_\parallel^*}\right)\\ &\quad + c\frac{\delta n_\mathrm{e}}{B_\parallel^{*2}}\boldsymbol{b}_0\times\nabla B_0\cdot\nabla\delta\phi + \frac{c\delta n_\mathrm{e}}{B_\parallel^{*2}}\nabla\times\boldsymbol{B}_0\cdot\nabla\delta\phi\Bigg]_\mathrm{NL} = 0.\end{aligned} \tag{8}$$

The parallel vector potential equation can be derived from electron parallel force balance,

$$\begin{aligned}\frac{\partial\delta A_\parallel}{\partial t} =& -c\boldsymbol{b_0}\cdot\nabla\delta\phi + \frac{c}{n_{0\mathrm{e}}\mathrm{e}}\boldsymbol{b_0}\cdot\nabla\delta p_\mathrm{e} + \frac{c}{n_{0\mathrm{e}}e}\frac{\delta\boldsymbol{B}_\perp}{B_\parallel^*}\cdot\nabla p_{\mathrm{e}0}\\ &- \frac{\nu_{\mathrm{ei}}m_\mathrm{e}c}{n_{0\mathrm{e}}\mathrm{e}^2}\left(n_{0\mathrm{i}}q_\mathrm{i}\delta u_{\parallel\mathrm{i}} - n_{0\mathrm{e}}\mathrm{e}\delta u_{\parallel\mathrm{e}}\right),\end{aligned} \tag{9}$$

where $n_{0\mathrm{e}}$ and δn_e, are the equilibrium and perturbed electron density, respectively. $\delta u_{\parallel\mathrm{i}}$ and $\delta u_{\parallel\mathrm{e}}$ are the perturbed parallel fluid velocity of ion and electron, respectively. $\delta v_{*\mathrm{e}}$ is the perturbed diamagnetic drift velocity for the electrons,

$$\delta\boldsymbol{v_{*e}} = -\frac{c}{n_{0\mathrm{e}}\mathrm{e}B_\parallel^*}\boldsymbol{b}_0\times\nabla\left(\delta p_{\perp\mathrm{e}} + \delta p_{\parallel\mathrm{e}}\right),$$

where $\delta p_{\perp\mathrm{e}}$ and $\delta p_{\parallel\mathrm{e}}$ are the perturbed electron pressure in the direction of perpendicular and parallel to equilibrium magnetic field, respectively. In equation (8), the first six terms are linear terms, and the fourth and sixth terms are geometry related. The terms with subscript 'NL' in equation (8) are nonlinear terms. When deriving equation (9), the electron inertial terms have been neglected and the collisional operators has been applied to the right-hand side of equation (1) with ν_{ei} the electron–ion collision frequency [29]. Thus the resistivity obeys the relation $\eta = \nu_{\mathrm{ei}}m_\mathrm{e}/\left(n_{0\mathrm{e}}\mathrm{e}^2\right)$.

The perturbed electron parallel velocity $\delta u_{\parallel\mathrm{e}}$ is calculated using the Ampere's law,

$$\delta u_{\parallel\mathrm{e}} = \tfrac{1}{n_{0\mathrm{e}}\mathrm{e}}\left(n_{0\mathrm{i}}q_\mathrm{i}\delta u_{\parallel\mathrm{i}} + \tfrac{c}{4\pi}\nabla_\perp^2\delta A_\parallel + \delta j_{\mathrm{bs}}\right), \tag{10}$$

where the perturbed ion parallel velocity can be obtained from the ion perturbed distribution function,

$$\delta u_{\parallel\mathrm{i}} = \frac{1}{n_{0\mathrm{i}}}\int v_\parallel\delta f_\mathrm{i}d\boldsymbol{v}.$$

Here we use equilibrium ion mass flow as the reference frame so the bootstrap current is carried by electrons. The $\delta u_{\parallel\mathrm{e}}$ represents the resistive (Ohmic) current part of the electron fluid velocity. The last term in equation (10) represents the

crucial neoclassical effects coming from the bootstrap current, which is implemented using the conventional formula [38],

$$\delta j_{\rm bs} = -1.46\frac{\sqrt{\epsilon}}{B_\theta}\frac{\partial \delta p}{\partial r}\ . \tag{11}$$

Here, B_θ is the poloidal magnetic field, $\epsilon = r/R_0$ is the local inverse aspect ratio, with r the local minor radius, R_0 the major radius. Without this term, the model reduces to classical TM model, which has previously been implemented and verified in the GTC [29]. In our simulations, this term can be switched on and off to study the bootstrap current effect. To recover the pressure flattening effect inside the island, a pressure diffusion equation is included as follows:

$$\begin{aligned}\frac{\partial \delta p}{\partial t} =& \chi_\parallel \nabla_\parallel^2 \delta p + \chi_\parallel \nabla_\parallel \left(\frac{\delta \boldsymbol{B}_\perp}{B_0}\cdot\nabla p_0\right) + \chi_\perp \nabla_\perp^2 \delta p \\ &+ \chi_\parallel \left[\frac{\delta \boldsymbol{B}_\perp}{B_0}\cdot\nabla\left(\nabla_\parallel \delta p + \frac{\delta \boldsymbol{B}_\perp}{B_0}\cdot\nabla\delta p + \frac{\delta \boldsymbol{B}_\perp}{B_0}\cdot\nabla p_0\right)\right. \\ &\left. + \nabla_\parallel\left(\frac{\delta \boldsymbol{B}_\perp}{B_0}\cdot\nabla\delta p\right)\right]_{\rm NL},\end{aligned} \tag{12}$$

where $\nabla_\parallel$ and $\nabla_\perp$ are the gradient operators defined along the equilibrium magnetic field, and $\chi_\perp$ and $\chi_\parallel$ are the perpendicular and parallel thermal diffusivity, respectively. Again the last four terms with subscript 'NL' are the nonlinear terms. Equations (11) and (12) constitute a rough model of the neoclassical bootstrap current effect, and are not self-consistently coupled with other equations. In principle, both electron and ion contributions to the perturbed bootstrap current can be included in equation (11), $\delta p = \delta p_{\rm i} + \delta p_{\rm e}$. However, we neglect the ion contribution to the perturbed bootstrap current in the current simulations for verification with the MHD theory and the simulations of other MHD codes. A self-consistent calculation of the perturbed pressure has been implemented in GTC [39], which will be utilized in the future simulations. The self-consistent calculations of the perturbed bootstrap current [40] will be implemented in future study.

Poisson's equation, which includes gyrokinetic ions and fluid electrons, takes the form

$$\left(1+\frac{\omega_{\rm pi}^2}{\Omega_{\rm i}^2}\right)\nabla_\perp^2\delta\phi = 4\pi\left(q_{\rm i}\delta n_{\rm i} - {\rm e}\delta n_{\rm e}\right), \tag{13}$$

where $\omega_{\rm pi} = 4\pi n_{0{\rm i}} q_{\rm i}^2/m_{\rm i}$ is the ion plasma frequency, and $\delta n_{\rm i}$ is the gyro-averaged perturbed ion gyrocenter density [41, 42],

$$\delta n_{\rm i} = \int \delta f_{\rm i} d\boldsymbol{v}.$$

Finally, equations (2)–(13) form a closed electromagnetic system for NTM simulations that includes the kinetic effects of ions.

2.3. Reduction to MHD limit

As the first step in verifying our NTM simulation model we show that our gyrokinetic model in the long-wavelength limit recovers the reduced MHD model. By integrating equation (7) in velocity space, we obtain the following continuity equation for ions:

$$\begin{aligned}&\frac{\partial \delta n_i}{\partial t} + \boldsymbol{B}_0\cdot\nabla\left(\frac{n_{0i}\delta u_{\parallel i}}{B_\parallel^*}\right) + B_0 \boldsymbol{v}_{\boldsymbol{E}}\cdot\nabla\left(\frac{n_{0i}}{B_\parallel^*}\right) \\ &\quad + \delta\boldsymbol{B}_\perp\cdot\nabla\left(\frac{n_{0i}u_{\parallel 0i}}{B_\parallel^*}\right) + \frac{c\nabla\times\boldsymbol{b}_0}{q_i}\cdot\nabla\left(\frac{\delta p_i}{B_\parallel^*}\right) \\ &\quad + \frac{c\boldsymbol{b}_0\times\nabla B_0}{q_i}\cdot\nabla\left(\frac{\delta p_i}{B_\parallel^{*2}}\right) + \frac{c\nabla\times\boldsymbol{b}_0\cdot\nabla B_0}{q_i B_\parallel^{*2}}\delta p_i \\ &\quad + \frac{c\nabla\times\boldsymbol{b}_0}{B_\parallel^*}\cdot n_{0i}\nabla\delta\phi + \delta\boldsymbol{B}_\perp\cdot\nabla\left(\frac{n_{0i}\delta u_{\parallel i}}{B_\parallel^*}\right) = 0.\end{aligned} \tag{14}$$

Next, we assume the ions and electrons have the same charge, $q_{\rm i} = -q_{\rm e} = {\rm e}$, and the equilibrium quasineutrality is enforced, $n_{0{\rm i}} = n_{0{\rm e}} = n_0$. We also define the perturbed charge density, perturbed Ohmic current and the perturbed fluid pressure as $\delta\rho \equiv {\rm e}\left(\delta n_{\rm i} - \delta n_{\rm e}\right)$, $\delta j_{\parallel{\rm ohm}} \equiv n_0{\rm e}\left(\delta u_{\parallel{\rm i}} - \delta u_{\parallel{\rm e}}\right)$ and $\delta p = \delta p_{\rm i} + \delta p_{\rm e}$, respectively. Combining equations (8) and (14), we obtain

$$\begin{aligned}&\frac{\partial\delta\rho}{\partial t} + B_0\cdot\nabla\left(\frac{\delta j_{\parallel{\rm ohm}}}{B_\parallel^*}\right) + \delta\boldsymbol{B}_\perp\cdot\nabla\left(\frac{j_{\parallel{\rm ohm}0}}{B_\parallel^*}\right) \\ &\quad + c\nabla\times\boldsymbol{b}_0\cdot\nabla\left(\frac{\delta p}{B_\parallel^*}\right) + c\boldsymbol{b}_0\times\nabla B_0\cdot\nabla\left(\frac{\delta p}{B_\parallel^{*2}}\right) \\ &\quad + \frac{c\nabla\times\boldsymbol{b}_0\cdot\nabla B_0}{B_\parallel^{*2}}\delta p + \left[\delta\boldsymbol{B}_\perp\cdot\nabla\left(\frac{\delta j_{\parallel{\rm ohm}}}{B_\parallel^{*2}}\right)\right]_{\rm NL} = 0.\end{aligned} \tag{15}$$

Again the last term with subscript 'NL' is the nonlinear term. We ignore the ion flow in the MHD limit, i.e. this model is performed in the plasma frame ignoring the flow shear effects. In the MHD limit, the parallel vector potential equation is simplified to

$$\begin{aligned}\frac{\partial\delta A_\parallel}{\partial t} =& -c\boldsymbol{b}_0\cdot\nabla\delta\phi + \frac{c}{n_0{\rm e}}\boldsymbol{b}_0\cdot\nabla\delta p_{\rm e} + \frac{c}{n_0{\rm e}}\frac{\delta\boldsymbol{B}_\perp}{B_\parallel^*}\cdot\nabla p_{\rm e0} \\ &- c\eta\delta j_{\parallel{\rm ohm}}.\end{aligned} \tag{16}$$

The Ampere's law can be simplified as

$$\delta j_{\parallel{\rm ohm}} = -\frac{c}{4\pi}\nabla_\perp^2\delta A_\parallel - \delta j_{\rm bs}\ . \tag{17}$$

The Poisson equation in the long-wavelength limit takes the following form,

$$\frac{\omega_{\rm pi}^2}{\Omega_{\rm i}^2}\nabla_\perp^2\delta\phi = -4\pi\,\delta\rho\ . \tag{18}$$

Finally, equations (15)–(18) with (11) and (12) form a close system for MHD simulations of NTMs.

3. MHD simulations in a cylindrical geometry

3.1. Equilibrium settings

In tokamak discharges, the $m/n = (2,1)$ and $(3,2)$ TMs are often the most dangerous macroscopic MHD instabilities, where m and n are the poloidal and toroidal harmonics, respectively. To validate the ability of GTC to simulate NTMs, we choose the HL-2A discharge #11727, which is heated by electron cyclotron resonance wave. As reported in [43], this discharge experiences successive sawtooth crashes starting from 740 ms, with $m/n = (1,1)$ precursors coupling to small scale $m/n = (2,1)$ modes. This produces a seed island for the NTM, which then nonlinearly saturates at a high level. The magnetic surface of the HL-2A is nearly circular, so we use this case to verify our model in a cylindrical geometry with a circular cross-section and with an imposed neoclassical bootstrap current defined by equation (11). Future studies will incorporate self-consistent neoclassical effects.

Figure 1 displays the equilibrium profiles of safety factor q and the normalized pressure, obtained from EFIT reconstruction, for the selected HL-2A discharge. The basic parameters of this discharge include an on-axis toroidal magnetic field of $B_0 = 1.27$ T, major radius $R_0 = 1.65$ m, minor radius $a = 0.4$ m, the position of the $q_s = 2$ surface at $r_s = 0.14R_0$, and an on-axis electron density and temperature of $n_{eq}(0) = 1.1 \times 10^{19} \mathrm{m}^{-3}$ and $T_{e,eq}(0) = 0.9$ keV, respectively, resulting an on-axis pressure ratio $\beta = 0.0025$ and a local poloidal beta at r_s of $\beta_p \equiv 8\pi^2 p/B_{ps}^2 = 0.172$. In the MHD simulations, the cold ions is employed, i.e. $T_{i,eq} \to 0$. The growth rates of TMs or NTMs is closely related to resistivity, and for high-temperature tokamak experiment, the resistivity η is typically less than $10^{-7}\Omega \cdot \mathrm{m}$. As for this equilibrium, the classical Spitzer resistivity is $\eta_{Sp} \sim 3 \times 10^{-8}\Omega \cdot \mathrm{m}$. However, η is set to $9 \times 10^{-6}\Omega \cdot \mathrm{m}$ in this work to reduce computational costs. Thermal diffusivity measurements for the current HL-2A discharge are not available. Theoretical calculations yield classical parallel thermal diffusivity $\chi_\parallel = 5.0 \times 10^9 \mathrm{m}^2\,\mathrm{s}^{-1}$ and neoclassical perpendicular thermal diffusivity $\chi_\perp = 5.5 \times 10^{-2} \mathrm{m}^2\,\mathrm{s}^{-1}$. However, the perpendicular diffusivity measured in experiments is often dominated by turbulent transport, which is much higher than the neoclassical transport. Notably, recent high-temperature experiments conducted on JT-60U [44] and DIII-D [45] tokamaks have shown a reduction of 1–2 orders in perpendicular thermal diffusivity inside a magnetic island compared to the background plasma transport. As a result, a perpendicular thermal conductivity $\chi_\perp \sim 1 \times 10^{-1} \mathrm{m}^2\,\mathrm{s}^{-1}$ has been observed. While a large thermal diffusivity ratio of $\chi_\parallel/\chi_\perp > 10^{10}$ may seem appropriate, it can lead to numerical issues during simulations. Consequently, we have opted for a more conservative ratio of $\chi_\parallel/\chi_\perp \leqslant 10^8$ in our current study, which may not be consistent with the measurements of HL-2A but would be reasonable for Ohmically heated plasmas [46]. In future study, these transport coefficients will be self-consistently calculated in gyrokinetic simulations.

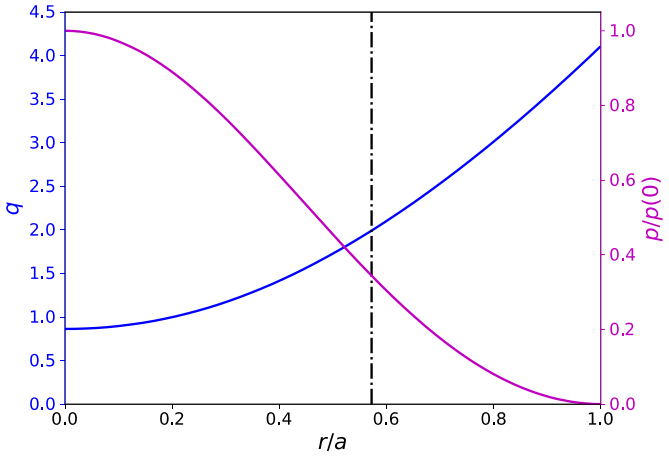

Figure 1. Radial profiles of the equilibrium safety factor q and normalized pressure. Also shown is the $q = 2$ flux surface position.

According to eigenvalue analysis [31], the classical TM stability index for this equilibrium profile,

$$r_s \Delta' \equiv \frac{1}{\delta\psi} \frac{\partial \delta\psi}{\partial r}\bigg|_{r_s-}^{r_s+} \approx -0.54 \ . \tag{19}$$

The effect of the second radial derivative of the current density at the resonant surface was also included for improving its accuracy [47]. The cylindrical geometry was employed to compute Δ', so the toroidicity effect was neglected in view of the large aspect ratio of the equilibrium under study [48]. The negative value of Δ' indicates the intrinsically stable nature of the classical $(2,1)$ TM for this equilibrium, resulting in a theoretical growth rate of $\tau_R \mathrm{d}\ln w/\mathrm{d}t = -44.3$. Here w is the island width, and $\tau_R = 4\pi r_s^2/\eta$ is the resistive diffusion time.

3.2. Verification against MRE in the small island limit

We first verify the MHD model, i.e. equations (15)–(18) with (11) and (12) by switching off and on the bootstrap current term in our simulations. The perpendicular thermal transport coefficient $\chi_\perp$ is set to $1\,\mathrm{m}^2\,\mathrm{s}^{-1}$, and the parallel thermal transport coefficient $\chi_\parallel$ is set to $1 \times 10^8 \mathrm{m}^2\,\mathrm{s}^{-1}$, resulting the scale island width [46], $w_d = 0.128 r_s$. In GTC simulations, we do not directly simulate the evolution of the island width w. Rather, it is reflected by the perturbed parallel vector potential $\delta A_\parallel$, which can be related to the island width,

$$w = 4\sqrt{\frac{R_0 q_s}{B_0 s_s}\left|\delta A_\parallel\right|}, \tag{20}$$

with $s_s = r_s(q'/q)_s$ the local magnetic shear on the rational flux surface. We perform simulations by applying a small perturbation to $\delta A_\parallel$, resulting in a small island width of $w = 0.01 r_s \ll w_d$. The growth rate of the island width is measured once a stable mode structure is obtained. We retain only the lowest 5 harmonics ($m = 0, 1, 2, 3, 4; n = 0, 2, 4, 6, 8$) in our simulations, as higher harmonics have been found to

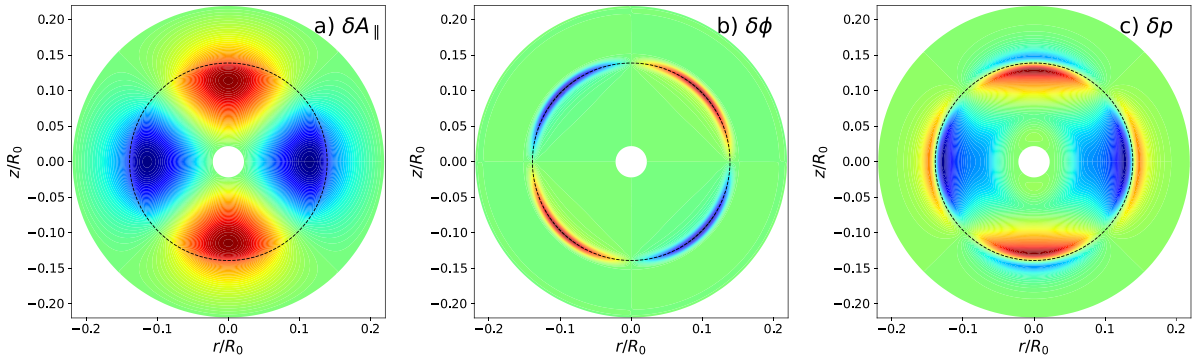

Figure 2. Snapshots of (a) $\delta A_\parallel$, (b) $\delta\phi$, and (c) δp mode structures of an NTM from the GTC MHD simulation, with the dashed line marking $q = 2$ surface position.

have smaller amplitudes. When the bootstrap current is not included, the simulated classical TM growth rates is

$$\tau_R \mathrm{d}\ln w/\mathrm{d}t = -45.8,$$

in excellent agreement with the theoretical result of 44.3. In contrast, when the bootstrap current is included in the simulation, the growth rate is

$$\tau_R \mathrm{d}\ln w/\mathrm{d}t = 15.0.$$

This positive growth rate indicates that the presence of the bootstrap current effect renders the mode unstable. To the best of the author's knowledge, this is the first reported simulation in which an inherently stable TM is used to verify the NTM model. Figure 2 displays the simulated NTM poloidal mode structure of $\delta A_\parallel$, $\delta\phi$, and δp, revealing a distinct $m = 2$ mode structure.

Next we verify the simulation model against the modified Rutherford theory in the small island limit. The growth of the NTM island width w is described by MRE, expressed as [46]

$$I_1 \frac{\tau_R}{r_s}\frac{\mathrm{d}w}{\mathrm{d}t} = r_s\Delta'(w) + 4.63\sqrt{\epsilon_s}\beta_p \frac{L_q}{L_p}\frac{r_s w}{w^2+w_d^2}, \qquad (21)$$

where the first term represents the classical TM contribution, the second term describes the neoclassical bootstrap current drive, $I_1 = 0.8227$ is a constant, and L_q and L_p denote the gradient scale lengths of the q profile and pressure profile, respectively. $w_d \propto \left(\chi_\perp/\chi_\parallel\right)^{1/4}$ is anti-proportional to the degree of pressure flattening inside the island. This MRE model is simplified, as several contributions from curvature effects, polarization current effects, and finite Larmor radius (FLR) effects have been neglected. The curvature effects [48–50] arising from toroidicity are neglected here because the aspect ratio is sufficiently large, and we aim to verify the model's accuracy for MRE in the cylindrical geometry. Furthermore, the polarization current effects and FLR effects [51–53] are ignored since we are assessing our simulation results using the MHD model. In small island limit of $w \ll w_d$, equation (21) reduces to [46, 54]

$$I_1 \frac{\tau_R}{r_s}\frac{\mathrm{d}w}{\mathrm{d}t} = r_s\Delta' \frac{w}{\delta} + 4.63\sqrt{\epsilon_s}\beta_p \frac{L_q}{L_p}\frac{r_s w}{w_d^2}, \qquad (22)$$

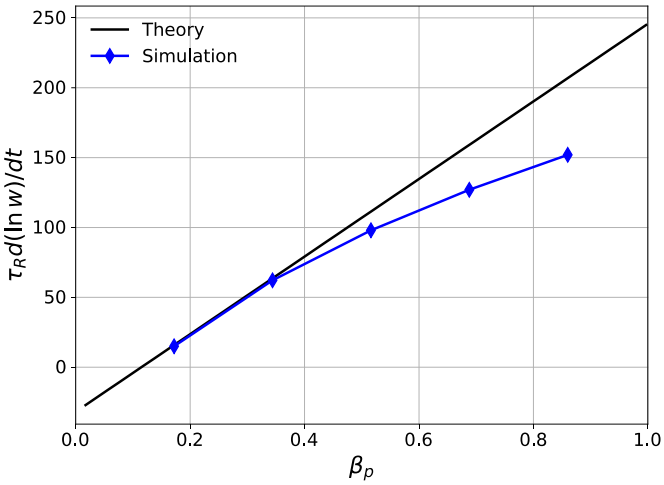

Figure 3. Dependence of the NTM growth rate in the small island limit on β_p. The black lines are calculated using equation (22).

where $\delta \propto \eta^{2/5}$. Substituting this scaling of δ into equation (22) gives the scaling of the dispersion relation $\tau_R \mathrm{d}\ln w/\mathrm{d}t \propto \left(c_1\eta^{3/5} + c_2\beta_p\eta\right)$, where c_1 and c_2 are constants depending only on the equilibrium quantities. The classical $(2,1)$ TM growth rate has been verified to scale as $\eta^{3/5}$ in previous studies [29, 31]. The growth rate of NTM island $\tau_R \mathrm{d}\ln w/\mathrm{d}t$ should be proportional to β_p, which determines the ratio of the bootstrap current to the total current. As the bootstrap current increases, the q-profile may change. However, considering a fixed q-profile is reasonable in order to understand the stability of an NTM against β_p and to benchmark the results of GTC with the theory. This linear dependence of the growth rate $\tau_R \mathrm{d}\ln w/\mathrm{d}t$ on β_p is valid as long as the profile of the safety factor q and the normalized profile of the pressure remain unchanged.

The theoretical scaling and simulation results are presented in figure 3. The β_p is increased by folding the central electron density $n_{eq}(0)$ while keeping the radial profiles of q, $n/n_{eq}(0)$ and $T_e/T_{eq}(0)$ fixed in these cases. The theoretical lines are obtained from equation (22) using the $\Delta\prime$ from equation (19), and all growth rates are normalized with respect to τ_R^{-1}. The GTC results reproduce the scaling between $\tau_R \mathrm{d}\ln w/\mathrm{d}t$ and β_p

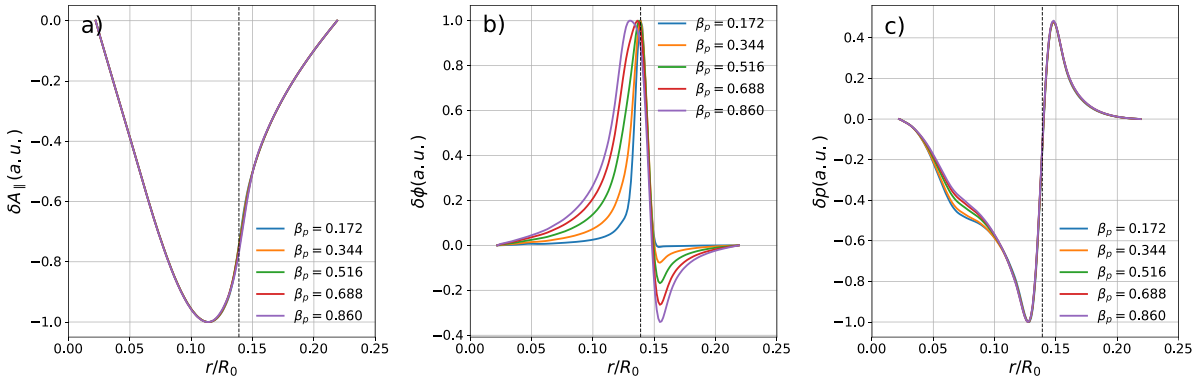

Figure 4. Radial mode structures of (a) $\delta A_\parallel$, (b) $\delta\phi$, and (c) δp for different β_p from GTC simulations of NTM for various plasma pressures.

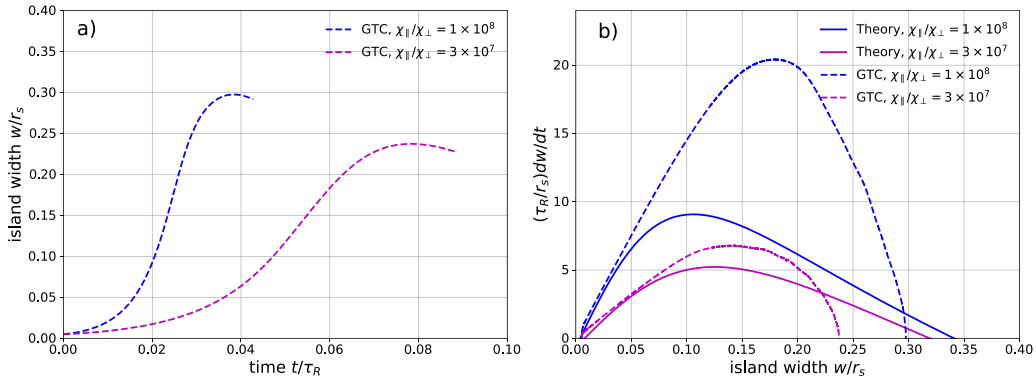

Figure 5. (a) Island width w grows history during the whole nonlinear simulation; (b) nonlinear growth $\mathrm{d}w/\mathrm{d}t$ versus the island width for $\chi_\parallel/\chi_\perp = 1\times10^8, 3\times10^7$, respectively. The theoretical results from equation (21) are also shown in solid lines.

in the small β_p limit, demonstrating a quantitative agreement between the simulations and the modified Rutherford theory. However, as β_p increases, the simulation results yield a smaller growth rate than that predicted by the MRE. The discrepancy between the simulations and the theoretical predictions at large β_p arises because the stabilizing effect of field line curvature from cylindrical geometry becomes non-negligible as β_p increases from 0.172 to 0.860 [55]. For the case of $\beta_\mathrm{p} = 0.172$, the plasma pressure ratio $\beta = 0.0025$. The simulated island growth rate is measured at $w/r_\mathrm{s} = 0.01 \gg \beta$, where the stabilizing effect of field line curvature of cylindrical geometry is negligible. On the other hand, for the case of $\beta_\mathrm{p} = 0.860$, the plasma pressure ratio $\beta = 0.0125$. The simulated island growth rate is also measured at $w/r_\mathrm{s} = 0.01 \sim \beta$, where the stabilizing effect of field line curvature of cylindrical geometry becomes non-negligible. However, we use a value of Δ' from equation (19) that accounts for the curvature effect of field line from cylindrical geometry for all β_p cases when plotting the theoretical scaling law according to equation (22).

Figure 4 shows the radial mode structures of $\delta A_\parallel$, $\delta\phi$ and δp in small island limits for these different β_p cases. Every curve in figure 4 is measured at an island width of $w \approx 0.01 r_\mathrm{s}$ and is normalized to its maximum value. As shown in figures 4(a) and (c), the radial mode structures of the parallel vector potential $\delta A_\parallel$ and pressure perturbation δp change very little as β_p increases. However, in figure 4(b), the radial mode structure of the electrostatic potential $\delta\phi$ changes significantly. First, the mode structure becomes broader as β_p increases. Second, the peak of the $\delta\phi$ profile gradually moves inward. In addition, $\delta\phi$ tends to be more negative outside the rational surface for a higher poloidal beta β_p. These features coincide with those reported by Sato and Wakatani [56].

3.3. Nonlinear evolution of NTM islands

As shown in equation (21), the destabilizing effect of bootstrap current term initially increases with island width, reaching a maximum value at $w \cong w_\mathrm{d}$, and then starts to decrease. Additionally, the classical term has a quasilinear dependence on the island width given by $\Delta'(w) = \Delta' - \alpha w$, where α is a parameter determined by the mode number and the equilibrium current density profile [57]. These two effects together lead to a finite saturated width of the NTM island. To save computational costs, we choose the case with $\beta_\mathrm{p} = 0.860$ as an example, which has the largest growth rate in the small island limit. Figure 5(a) shows the evolution of island width w during the entire nonlinear simulation for two cases, $\chi_\parallel/\chi_\perp = 1\times10^8$ and 3×10^7, respectively. The NTM island grows to a saturation level of $0.3r_\mathrm{s}$ and $0.24r_\mathrm{s}$, respectively. The dependence of the island growth, $\mathrm{d}w/\mathrm{d}t$, on the island size w for these two cases is shown in figure 5(b). The theoretical result from equation (21) is also plotted for comparison with the quasilinear dependence of Δ' on the island width, $\Delta'(w) = \Delta' - \alpha w$ [57]. Although the maximum island

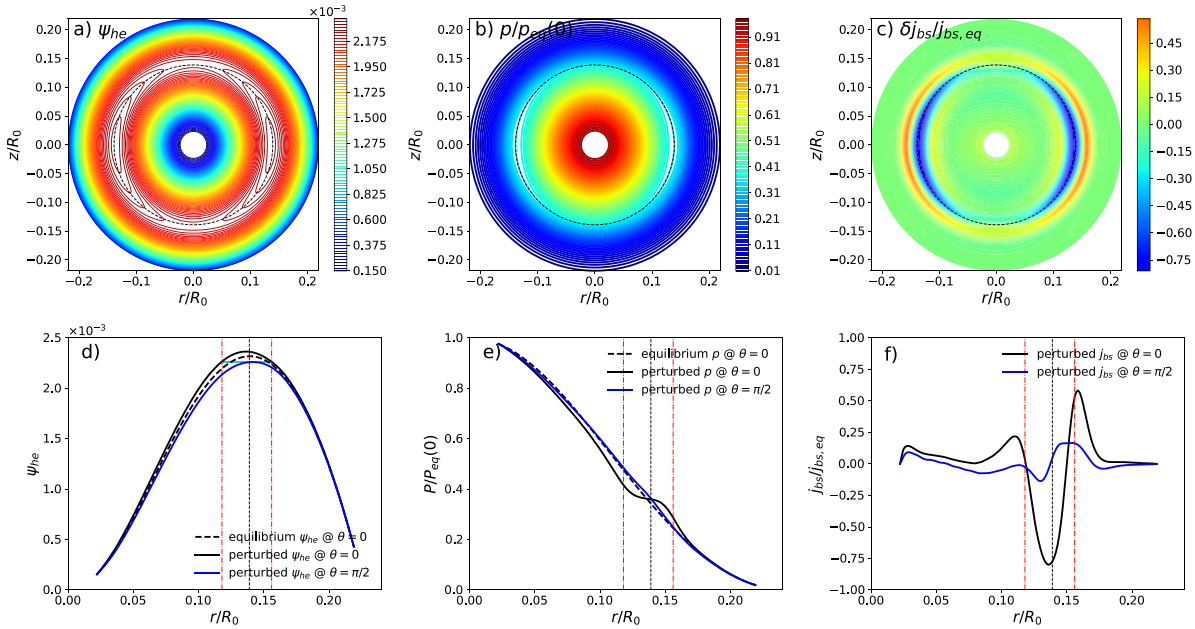

Figure 6. Contours at $\zeta = 0$ poloidal plane (a)–(c) and radial profiles at low field side (d)–(f) of the helical flux, normalized pressure, and perturbed bootstrap current when $w = 0.25r_s$ for the $\chi_\parallel/\chi_\perp = 1 \times 10^8$ case. (a) ψ_{he}; (b) normalized pressure $p/p_{eq}(0)$; (c) normalized perturbed bootstrap current $\delta j_{bs}/j_{bs,eq}$; (d) radial profile of the equilibrium and perturbed ψ_{he}; (e) radial profile of the normalized pressure $p/p_{eq}(0)$; (f) radial profile of the perturbed part of bootstrap current $\delta j_{bs}/j_{bs,eq}$. The thin black dashed line represents $q = 2$ surface for all panels. The shadowed region bounded by red dashed lines shows the island separatrix for panels (d)–(f).

growth of our result is almost twice of the MRE prediction for the $\chi_\parallel/\chi_\perp = 1 \times 10^8$ case, the final saturated island width between GTC and MRE agrees well. For the $\chi_\parallel/\chi_\perp = 3 \times 10^7$ case, a good agreement between GTC and MRE can be found for both the maximum growth and saturation level.

Now we show the pressure gradient flattening effects at large island. Figure 6 shows the contours at $\zeta = 0$ poloidal plane and radial profiles at low field side of the helical flux surfaces, normalized pressure and perturbed bootstrap current when the island width reaches $w = 0.25r_s$ for the $\chi_\parallel/\chi_\perp = 1 \times 10^8$ case. The helical flux surfaces are calculated as follows,

$$\psi_{he} = \psi - \frac{\psi_t}{q_s} - g\delta A_\parallel,$$

with ψ and ψ_t the poloidal and toroidal flux, respectively. In figure 6(a), we observe a clear $(2,1)$ island from the contours of ψ_{he} at the poloidal plan $\zeta = 0$. The island separatrix is identified based on the radial profiles passing through the O point ($\theta = 0$) and X point ($\theta = \pi/2$) and is depicted as a shadowed region in figures 6(d)–(f). The contours and radial profiles of normalized pressure $p/p_{eq}(0)$ are shown in figures 6(b) and (e). As anticipated, the pressure profile near the $q = 2$ surface is flattened inside the island, with a significantly flattening observed across the O point while remaining present across the X point. This pressure flattening effects also lead to the vanishing of bootstrap current within the island and its accumulation along the separatrix, which can be seen in figures 6(c) and (f).

4. Toroidal geometry simulations in the small island limit using MHD model

Implementing the MHD model in the toroidal geometry, we can investigate the behavior of NTM in the realistic tokamak geometry. As a verification of the code capability, we consider the simplest concentric tokamak for the MHD simulation of the $(2,1)$ NTM. By using the same parameters as those in the cylindrical geometry and keeping the toroidal magnetic field curvature and gradient, we obtain the mode structure of the $(2,1)$ NTM in figure 7 from the tokamak simulation. A comparison with the counterpart in the cylindrical geometry shown in figure 2 reveals that the mode structures of perturbed $\delta A_\parallel, \delta\phi, \delta p$ in tokamak geometry exhibit a slight 'squeezing' towards the high-field-side (left side). The small breaking of left-right symmetry can be attributed to the relative large aspect ratio in our case, $R_0/r_s = 7.18$.

In order to investigate the influence of toroidal effects on the growth rate of NTM at different pressure ratios, we re-simulated the cases shown in figure 3 under tokamak configuration using the same MHD model. The results in tokamak geometry are shown in figure 8. These growth rates are measured at an island width of $w \approx 0.01r_s$. The growth rate in tokamak geometry is slightly higher that in the cylindrical geometry, indicating a destabilizing effect of the toroidal geometry on the NTM. This appears to contradict the well-known GGJ effect [48, 49, 58]. This is probably because of the geometric modification of equilibrium magnetic field strength. The second order correction term of the magnetic field in the toroidal geometry is retained in our simulations:

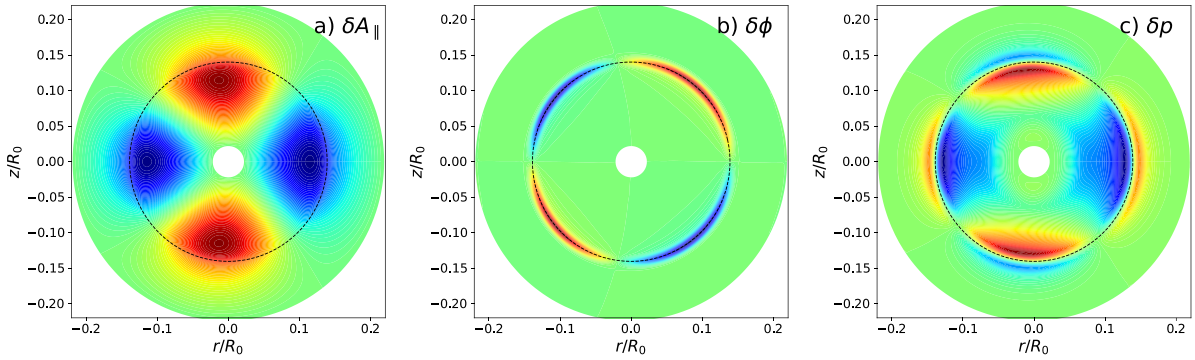

Figure 7. Snapshots of (a) $\delta A_\parallel$, (b) $\delta\phi$, and (c) δp mode structures of an NTM from the GTC fluid simulation in a tokamak geometry, with the dashed line marking $q = 2$ surface position.

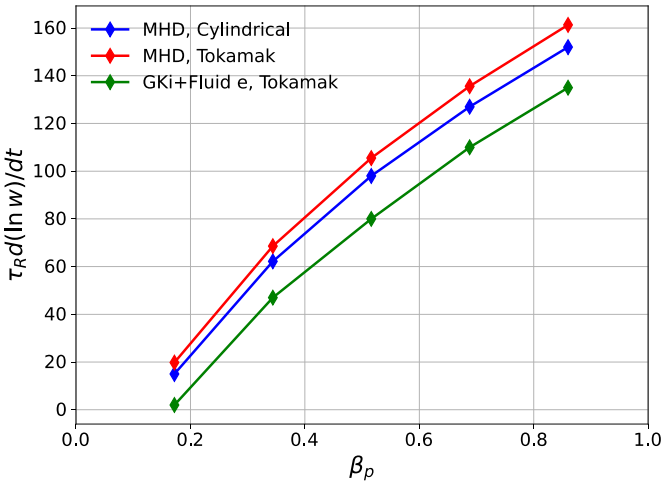

Figure 8. Comparison of the dependence of the NTM growth rate in the small island limit on β_p between cylindrical and tokamak geometry.

$$B_\zeta = \left[1 - \tfrac{r}{R_0}\cos\theta + \left(\tfrac{r}{R_0}\right)^2 \cos^2\theta\right] B_{\zeta 0}. \qquad (23)$$

This correction would lead to an increase of the radial derivative of equilibrium poloidal field B_p, and therefore an increase of the free energy for driving the classical TMs.

5. Gyrokinetic simulations in a toroidal geometry

The impact of thermal ion kinetic effects on the NTM stability threshold is well-established. Firstly, the FLR effect of thermal ions sets the length scale where the polarization current becomes relevant. When the island width w is comparable to the ion Larmor radius, ρ_Li, the different responses of ions and electrons to the rotating island give rise to an electrostatic potential, which could induce a polarization current contributing to the island evolution through the MRE [52,53]. Secondly, the finite banana-orbit width of trapped ions in toroidal geometry would also contribute to a net current, i.e. the neoclassical polarization current [59–61], that can affect the evolution of island when w is comparable to the ion banana width ρ_bi. Recently, Imada *et al* demonstrated that the pressure gradient can be maintained across the NTM island when w is comparable to the ion poloidal Larmor radius $\rho_{\theta\mathrm{i}}$, suppressing the bootstrap current drive for the NTM growth [33, 62].

A global gyrokinetic particle simulation approach for NTMs has been implemented in the GTC. By incorporating the perturbed distribution function of the kinetic ions, we can obtain the charge and current densities that arise due to thermal ions, which are then coupled into the Poisson equation and Ampere's law. Thus the thermal ion kinetic effects are incorporated into our NTM simulation model, as described by equations (2)–(13).

In order to quantify the kinetic effects of thermal ions, we perform gyrokinetic simulations using the same equilibrium parameters as in the MHD cases, while keeping the total pressure unchanged by setting the electron and ion temperature to $T_{\mathrm{e},eq}(0) = 850\,\mathrm{eV}, T_{\mathrm{i},eq}(0) = 50\,\mathrm{eV}$. The more realistic ion temperature will be simulated in the future study. These simulations are performed in the small island limit of the toroidal geometry, as well. Figure 8 also displays the growth rates obtained from these simulations, which are measured at an island width of $w \approx 0.01 r_\mathrm{s}$. The results demonstrates that the kinetic effects of thermal ions significantly reduce the NTM growth rates, indicating a stabilizing effect on the NTM stability. In fact, this effect is much stronger than the destabilizing effect of the toroidicity. For instance, in the case of $\beta_\mathrm{p} = 0.172$, the NTM changes from unstable to marginally stable due to the thermal ion kinetic effects. This suggests that these effects can increase the beta threshold for NTM excitation, thus improving the stability of tokamak plasmas. The main reason for the reduction of NTM growth rates is additional damping due to thermal ion kinetic effects including radiative damping and ion Landau damping arising from the finite parallel electric field. The decrease of the equilibrium electron pressure, which reduces the pressure gradient drive in equation (12), also partially contribute to the reduction of NTM growth rates. Although the large banana orbit width of thermal ions, ρ_bi, could contribute to a neoclassical polarization current when $\rho_\mathrm{bi} \gtrsim w$, especially for these cases $\rho_\mathrm{bi} = 0.027 r_\mathrm{s}$, this effect does not dominate the stabilizing regime because the ion parallel streaming frequency around the island is about $\omega \cong 8.4 \times 10^4 \mathrm{rad\,s^{-1}}$, much larger than the island rotation frequency. Moreover, the FLR effect of thermal

ions does not contribute significantly to the stabilization of NTMs, since the ion Larmor radius $\rho_{\mathrm{Li}} \ll w$ at such small T_{i}, as confirmed by our drift-kinetic ion simulation, although these results are not presented here.

The mode structures exhibit no significant change between the resistive MHD and the gyrokinetic simulations, except for a rotation in the ion diamagnetic direction in the gyrokinetic cases. However, it should be noted thatquantitative comparison between the simulated and experimental rotation frequencies is not meaningful due to the parameters (like the resistivity, the temperature and thermal diffusivities) used in the simulations for computational convenience, which may not accurately reflect the experimental conditions. Additionally, the application of a ECRH system in the HL-2A discharge may also contribute to mode rotation. Thus, we did not compare the simulated rotation frequency with experimental data. Further investigation is needed to fully understand the impact of kinetic effects of thermal ions on the NTM island evolution dynamics and saturation level. In earlier GTC simulations [63], we have observed turbulence reduction at the O-point for static magnetic islands. However, the interaction between turbulence and NTM islands is beyond the scope of this work.

6. Summary and conclusions

In this work, we have developed a gyrokinetic simulation model within the GTC framework that incorporates gyrokinetic ions and fluid electrons for the study of NTMs in a toroidal geometry. The neoclassical bootstrap current is introduced via a standard neoclassical model, and the pressure transport equation based on a diffusion model is included to close the system. We have verified our NTM simulation model by performing cylindrical geometry simulations in the MHD limit. Our results reveal that the neoclassical bootstrap current effect can destabilize an otherwise stable classical TM. Moreover, we have demonstrated that the NTM growth rate linearly increases with the poloidal beta β_p in the small island limit, in agreement with the modified Rutherford theory. Additionally, we observed good agreement with the modified Rutherford theory in terms of the saturation level and the maximum growth of the NTM island width during the nonlinear evolution dynamics. We also performed simulations in a toroidal geometry and found that toroidal effects can have a destabilizing effect on NTMs. Gyrokinetic simulations of NTMs in toroidal geometry show that the ions' kinetic effects can effectively reduce the NTM growth rate even with the destabilizing effect of toroidicity, underscoring the importance of thermal ions' kinetic effects in determining the threshold for NTM excitation.

This study presents an initial progress towards the first-principle kinetic simulations of NTMs in tokamaks. Nevertheless, the current model is limited by the absence of self-consistent treatment of certain neoclassical effects, as well as some key parameters such as turbulent thermal diffusivities, which may limit the generalizability of the results to tokamak discharges. To address these limitations, future research will aim to enhance the capabilities of the GTC code by implementing a comprehensive electron model, such as the conservative nonlinear electromagnetic simulation model [64, 65], to achieve self-consistent computation of the neoclassical bootstrap current and diffusivities driven by microturbulence, and thereby enable more accurate determination of the NTM threshold.

Data availability statement

All data that support the findings of this study are included within the article (and any supplementary files).

Acknowledgments

The authors gratefully acknowledge useful discussions with Dr Xiaoquan Ji, Dr Jian Bao, Dr Chao Dong and Dr Hao Shi. This work is supported by the National MCF Energy R&D Program under Grant Nos. 2018YFE0304100, 2018YFE0311300 and 2017YFE0301300; the National Natural Science Foundation of China under Grant Nos. 11675256, 11675257, 11835016, 11875067, 11905109, 11947238, 11705275 and 11847131; the Strategic Priority Research Program of the Chinese Academy of Sciences under Grant No. XDB16010300; the Key Research Program of Frontier Science of the Chinese Academy of Sciences under Grant No. QYZDJ-SSW-SYS016; the External Cooperation Program of the Chinese Academy of Sciences under Grant No. 112111KYSB20160039; the China Scholarship Council under Grant No. 202206010201, and by US DOE SciDAC ISEP Center. Resources from the National Supercomputer Center in Tianjin (NSCC-TJ), the Oak Ridge Leadership Computing Facility at Oak Ridge National Laboratory (OLCF) and the National Energy Research Scientific Computing Center (NERSC) were used in this research.

ORCID iDs

Shuying Sun https://orcid.org/0000-0002-3991-872X
Wenlu Zhang https://orcid.org/0000-0002-7136-2119
Zhihong Lin https://orcid.org/0000-0003-2007-8983
Xishuo Wei https://orcid.org/0000-0001-7486-0407
Pengfei Liu https://orcid.org/0000-0002-6739-3684

References

[1] Furth H P, Killeen J and Rosenbluth M N 1963 *Phys. Fluids* **6** 459–84
[2] Rutherford P H 1973 *Phys. Fluids* **16** 1903
[3] Qu W X and Callen J D 1985 *University of Wisconsin Report* No. UWPR85 5
[4] Carrera R, Hazeltine R D and Kotschenreuther M 1986 *Phys. Fluids* **29** 899
[5] Chang Z, Callen J D, Fredrickson E D, Budny R V, Hegna C C, McGuire K M and Zarnstorff M C (TFTR group) 1995 *Phys. Rev. Lett.* **74** 4663–6

[6] de Vries P C, Johnson M F, Alper B, Buratti P, Hender T C, Koslowski H R and Riccardo V 2011 *Nucl. Fusion* **51** 053018
[7] Buttery R J *et al* 2000 *Plasma Phys. Control. Fusion* **42** B61–73
[8] La Haye R J 2006 *Phys. Plasmas* **13** 055501
[9] Wilson H R 2006 *Fusion Sci. Technol.* **49** 155–63
[10] Yu Q and Günter S 1998 *Phys. Plasmas* **5** 3924–8
[11] Lütjens H, Luciani J F and Garbet X 2001 *Plasma Phys. Control. Fusion* **43** A339–48
[12] Gianakon T A, Kruger S E and Hegna C C 2002 *Phys. Plasmas* **9** 536–47
[13] Wei L and Wang Z-X 2014 *Nucl. Fusion* **54** 043015
[14] Stratton B C *et al* 1999 *Nucl. Fusion* **39** 1309–19
[15] Poli E, García-Muñoz M, Fahrbach H-U and Günter S (ASDEX Upgrade Team) 2008 *Phys. Plasmas* **15** 032501
[16] García-Mũoz M *et al* 2009 *Nucl. Fusion* **49** 085014
[17] Li E *et al* 2016 *Plasma Phys. Control. Fusion* **58** 045012
[18] Takahashi R, Brennan D P and Kim C C 2009 *Phys. Rev. Lett.* **102** 135001
[19] Lin Z, Hahm T S, Lee W W, Tang W M and White R B 1998 *Science* **281** 1835–7
[20] Lin Z, Tang W M and Lee W W 1997 *Phys. Rev. Lett.* **78** 456–9
[21] Lin Z, Holod I, Chen L, Diamond P H, Hahm T S and Ethier S 2007 *Phys. Rev. Lett.* **99** 265003
[22] Zhang W, Lin Z and Chen L 2008 *Phys. Rev. Lett.* **101** 095001
[23] Zhang H S, Lin Z and Holod I 2012 *Phys. Rev. Lett.* **109** 025001
[24] Wang Z, Lin Z, Holod I, Heidbrink W W, Tobias B, Van Zeeland M and Austin M E 2013 *Phys. Rev. Lett.* **111** 145003
[25] Liu P, Wei X, Lin Z, Brochard G, Choi G J, Heidbrink W W, Nicolau J H and McKee G R 2022 *Phys. Rev. Lett.* **128** 185001
[26] Deng W, Lin Z and Holod I 2012 *Nucl. Fusion* **52** 023005
[27] McClenaghan J, Lin Z, Holod I, Deng W and Wang Z 2014 *Phys. Plasmas* **21** 122519
[28] Brochard G *et al* 2022 *Nucl. Fusion* **62** 036021
[29] Liu D, Zhang W, McClenaghan J, Wang J and Lin Z 2014 *Phys. Plasmas* **21** 122520
[30] Liu D, Bao J, Han T, Wang J and Lin Z 2016 *Phys. Plasmas* **23** 022502
[31] Shi H, Zhang W, Feng H, Lin Z, Dong C, Bao J and Li D 2019 *Phys. Plasmas* **26** 092512
[32] Holod I, Zhang W L, Xiao Y and Lin Z 2009 *Phys. Plasmas* **16** 122307
[33] Imada K, Wilson H R, Connor J W, Dudkovskaia A V and Hill P 2018 *Phys. Rev. Lett.* **121** 175001
[34] Dudkovskaia A V, Bardoczi L, Connor J W, Dickinson D, Hill P, Imada K, Leigh S, Richner N, Shi T and Wilson H R 2023 *Nucl. Fusion* **63** 016020
[35] Feng H, Zhang W, Dong C, Cao J and Li D 2017 *Phys. Plasmas* **24** 102125
[36] Brizard A J and Hahm T S 2007 *Rev. Mod. Phys.* **79** 421–68
[37] Parker S E and Lee W W 1993 *Phys. Fluids B: Plasma Phys.* **5** 77–86
[38] Hinton F L and Hazeltine R D 1976 *Rev. Mod. Phys.* **48** 239–308
[39] Liu P, Wei X, Lin Z, Brochard G, Choi G J and Nicolau J H 2023 *Rev. Mod. Plasma Phys.* **7** 15
[40] Dong G and Lin Z 2017 *Nucl. Fusion* **57** 036009
[41] Lee W W 1987 *J. Comput. Phys.* **72** 243–69
[42] Xiao Y, Holod I, Wang Z, Lin Z and Zhang T 2015 *Phys. Plasmas* **22** 022516
[43] Ji X-Q, Yang Q-W, Liu Y, Zhou J, Feng B-B and Yuan B-S 2010 *Chin. Phys. Lett.* **27** 065202
[44] Ida K, Kamiya K, Isayama A and Sakamoto Y 2012 *Phys. Rev. Lett.* **109** 065001
[45] Bardóczi L, Rhodes T L, Carter T A, Crocker N A, Peebles W A and Grierson B A 2016 *Phys. Plasmas* **23** 052507
[46] Fitzpatrick R 1995 *Phys. Plasmas* **2** 825–38
[47] Militello F and Porcelli F 2004 *Phys. Plasmas* **11** L13–16
[48] Kotschenreuther M, Hazeltine R D and Morrison P J 1985 *Phys. Fluids* **28** 294–302
[49] Glasser A H, Greene J M and Johnson J L 1975 *Phys. Fluids* **18** 875
[50] Lütjens H, Luciani J-F and Garbet X 2001 *Phys. Plasmas* **8** 4267–70
[51] Smolyakov A I 1989 *Sov. J. Plasma Phys.* **15** 667
[52] Waelbroeck F L, Connor J W and Wilson H R 2001 *Phys. Rev. Lett.* **87** 215003
[53] Connor J W, Waelbroeck F L and Wilson H R 2001 *Phys. Plasmas* **8** 2835–48
[54] Lütjens H and Luciani J-F 2002 *Phys. Plasmas* **9** 4837–40
[55] Biskamp D 1997 *Nonlinear Magnetohydrodynamics* (Cambridge University Press)
[56] Sato M and Wakatani M 2005 *Nucl. Fusion* **45** 143–9
[57] White R B, Monticello D A, Rosenbluth M N and Waddell B V 1977 *Phys. Fluids* **20** 800–5
[58] Glasser A H, Greene J M and Johnson J L 1976 *Phys. Fluids* **19** 567
[59] Poli E, Bergmann A and Peeters A G 2005 *Phys. Rev. Lett.* **94** 205001
[60] Poli E, Bottino A, Hornsby W A, Peeters A G, Ribeiro T, Scott B D and Siccinio M 2010 *Plasma Phys. Control. Fusion* **52** 124021
[61] Hornsby W A, Migliano P, Buchholz R, Kroenert L, Weikl A, Peeters A G, Zarzoso D, Poli E and Casson F J 2015 *Phys. Plasmas* **22** 022118
[62] Imada K, Wilson H R, Connor J W, Dudkovskaia A V and Hill P 2019 *Nucl. Fusion* **59** 046016
[63] Fang K S and Lin Z 2019 *Phys. Plasmas* **26** 052510
[64] Bao J, Liu D and Lin Z 2017 *Phys. Plasmas* **24** 102516
[65] Bao J, Lin Z and Lu Z X 2018 *Phys. Plasmas* **25** 022515